scientific reports

Check for updates

OPEN

The zinc bound form of the actinomycete derived natural product compound JBIR-141 induces a mitotic phenotype in fission yeast

Richard Alexander Lewis[1,2]✉, Jacqueline Hayles[3], Michael John Hall[4], Joe Gray[5], Sofanit Mebrate[3], Juanjuan Li[6], Nicholas Edward Ellis Allenby[1,7] & Jeff Errington[1,8]

This study was designed to identify the natural product compound produced by the actinomycete strain "S149" which is capable of inducing a strong small cell phenotype, called wee, in the fission yeast *Schizosaccharomyces pombe*. We purified the bioactive molecule, which, on the basis of mass spectrometry data, was identified as a novel zinc-bound form of the previously published molecule JBIR-141. JBIR-141 was not previously known to be a zincophore and does not possess structural features common to other bacterial zinc-binding natural product compounds. Testing the effect of the Zn^{2+} bound form of JBIR-14 against a series of *S. pombe* deletion mutants which express a wee phenotype suggested its potential target in fission yeast is either Pyp1, which is involved in regulation of the onset of mitosis, an important control in the eukaryotic cell cycle, or an element in the Pyp1 signalling pathway.

Keywords JBIR-141, Zinc, Zincophore, Fission yeast, Pyp1

Actinomycetes are soil dwelling, filamentous bacteria which have a complex life cycle, often comprising differentiation and sporulation. They are well known for their ability to synthesize a wide range of bioactive natural product compounds, many of which are of medical and commercial importance. To identify interesting compounds, we have used the fission yeast *Schizosaccharomyces pombe*, which is a rod-shaped unicellular eukaryote that grows by apical extension and divides by medial fission and septation[1] and is an excellent organism for genetic studies[2]. The genome has been sequenced[3] and there is a genome wide gene deletion collection available[4] making it a useful organism to identify morphological mutants and their cellular function[5]. The actinomycete strain S149, which induces a wee phenotype, was identified in a study where we described a novel screen for Actinomycete derived bioactive natural compounds using a microscopy-based approach, to determine their effect on *S. pombe* cellular morphology and to identify chemical entities affecting these processes[6].

In the original screen we identified 242 actinomycete bacterial strains which induced strong cell morphology phenotypes in *S. pombe*, which were classified into 8 major phenotypes. We have previously reported the identification of several known natural products (cycloheximide, streptonigrin, leptomycin) which induce various *S. pombe* morphological phenotypes[6] in addition to others (candicidin, streptothricin, fungichromin, filipin) which specifically induce a "rounded" phenotype[6,7]. However, Actinomycete strains capable of inducing a wee phenotype were of particular interest to us as a wee phenotype can be associated with premature entry

[1]Demuris Ltd/Odyssey Therapeutics, The Biosphere, Draymans Way, Newcastle Helix, Newcastle upon Tyne NE4 5BX, UK. [2]Axitan Ltd, 1 Arlington Court, Whittle Way, Stevenage SG1 2FS, UK. [3]Cell Cycle Laboratory, The Francis Crick Institute, 1 Midland Road, London NW1 1AT, UK. [4]Chemistry, School of Environmental and Natural Sciences, Newcastle University, Newcastle upon Tyne NE1 7RU, UK. [5]Pinnacle Laboratory, Institute for Cell and Molecular Biosciences, Newcastle University, Newcastle upon Tyne NE1 7RU, UK. [6]University of Southampton, University Road, Southampton SO17 1AT, UK. [7]John Dawson Drug Discovery and Development Research Institute, Faculty of Health Sciences & Wellbeing, University of Sunderland, Sunderland SR1 3SD, UK. [8]Faculty of Medicine and Health, University of Sydney, Biomedical Building C81, 3 Central Avenue, Eveleigh, Sydney NSW 2015, Australia. ✉email: r.lewis@axitan.com

into mitosis and division of cells at a small cell size. This phenotype is associated with a rate limiting process controlling the onset of mitosis and so is important for understanding cell cycle control[8].

Results & discussion

During the screen which identified S149 as a strain of interest, plugs cut from confluent lawns of S149 grown on GYM agar[9] were bioassayed against *S. pombe* SAK950[10] (as described below in "Experimental Procedures" 4.2) the *S. pombe* cells exhibited a wee cell phenotype, (length = ~ 10 µm at septation) which closely resembles *S. pombe* mutant cells advanced into mitosis[11]. Figure 1a illustrates untreated *S. pombe pmd1Δ* cells whilst Fig. 1b illustrates *S. pombe pmd1Δ* cells treated with the purified bioactive molecule from S149, which exhibit a wee cell phenotype. We hypothesised that S149 produced a bioactive natural product capable of specifically inhibiting a component of the cell cycle control mechanism acting over the onset of mitosis. As such a molecule would find utility as an experimental tool in a similar fashion to okadaic acid[12] we determined to purify and investigate the role of bioactive molecule produced by S149.

Purification of the bioactive natural product compound from S149

The 16 S rRNA sequence of S149 has been determined and the closest BLAST match is *Streptomyces coeruleofuscus* (GenBank: AB184840.1) with no mismatches over 1,413 nt. The physical appearance of S149 i.e. production of blue-green spores accompanied by production of dark brown pigmentation, is also consistent with the published description of *Streptomyces coeruleofuscus*[13].

Following medium optimisation a study of the natural product compound produced by S149 was found to be maximally produced when the strain was cultured for 2–3 days on Medium I agar plates. The bioactive molecule produced was purified as described below (see "Experimental Procedures" 4.5–4.9) with the bioactive fractions being identified *via S. pombe* bioassay and phenotypic assessment of the *S. pombe* cells in the halo.

The purified compound was analysed by HPLC and bioactivity (haloes visible after 16–24 h) found to be associated with three peaks designated 1–3 (Fig. 2a). Additionally, we identified a further peak, designated Peak 0, (Fig. 2a) which contained a closely related species, as determined by comparison of the u.v. absorbance spectra of Peaks 0–3, (Fig. 2b and c) but whose bioactivity against *S. pombe* was far slower to develop, and a less distinct halo was observed after 48–72 h. Material from the two major peaks- Peaks 0 and 1, was collected by "peak-picking" using the HPLC (as described in "Experimental Procedure" Sect. 4.9). When analysed by direct injection MS (and MS-MS) the Peak 1 material was found to contain the protonated species $m/z = 745.2735$ $[M+H^+]$ in addition to the sodium adduct $m/z = 767.2551$ $[M+Na^+]$ (Fig. 3a). However, Peak 0 contained a mixture of ions (Fig. 4a) with the two most abundant being $m/z = 683.3614$ $[M+H^+]$ and $m/z = 653.3655$ $[M+H^+]$, in addition to the minor ion at $m/z = 745.2755$ $[M+H^+]$. The Peak 0 $m/z = 745.2755$ $[M+H^+]$ species is identical to the $m/z = 745.2735$ $[M+H^+]$ already seen in Peak 1 (Fig. 3a). Moreover, it is clear from the MS-MS spectra, (Fig. 4b) that the $m/z = 745.2755$ $[M+H^+]$ ion generates the $m/z = 682.8996$ $[M+H^+]$ species (Fig. 4b), which is identical to the $m/z = 683.3614$ $[M+H^+]$ species seen in the MS (Fig. 4a). The MS-MS of the $m/z = 683.3614$ $[M+H^+]$ species generates the $m/z = 652.9787$ $[M+H^+]$ species (Fig. 4c) which is identical to the $m/z = 653.3655$ $[M+H^+]$ species seen in the MS (Fig. 4a).

We interpreted these data as the $m/z = 683.3614$ $[M+H^+]$ species as representing the S149 molecule of interest and the $m/z = 745.2755$ $[M+H^+]$ as being a Zn^{2+} bound form of the molecule. The mass difference between the $m/z = 745.2755$ $[M+H^+]$ and $m/z = 683.3614$ $[M+H^+]$ species is 61.9141, which is consistent with a loss of Zn^{2+} (mass = 63.929), and subsequent acquisition of two protons (mass = 1.007) by the S149 molecule, to maintain charge neutrality.

We also note that the $m/z = 745.2735$ $[M+H^+]$ species seen in Peaks 0–1 possesses a distinctive isotope pattern (Figs. 3a and 4a) which is not seen with the $m/z = 683.3614$ $[M+H^+]$ species (Figs. 3b and 4a). This provides additional evidence that the S149 molecule binds Zn^{2+} as the isotope pattern is consistent with the abundances of the natural isotopes of zinc (Zn^{64}: 49.17%, Zn^{66}: 27.73%, Zn^{67}: 4.04%, Zn^{68}: 18.56%, Zn^{70}: 0.61%) (Fig. 5b). The isotope pattern from the $m/z = 745.2735$ $[M+H^+]$ correlates with that generated using the formula

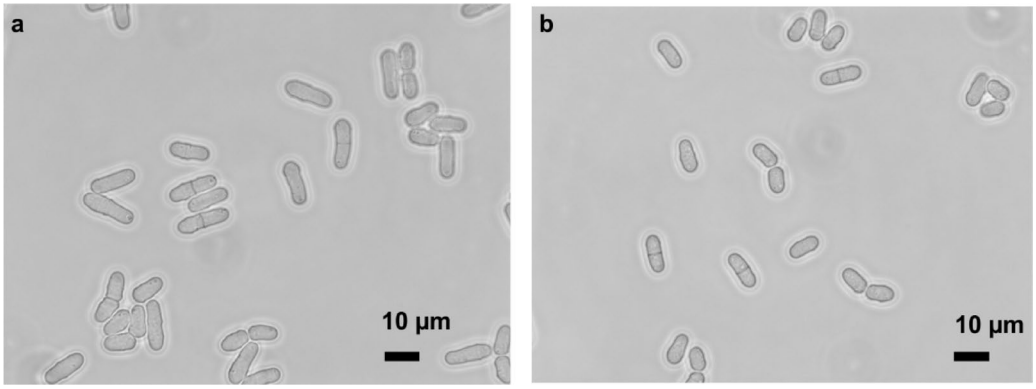

Fig. 1. (**a**) Images of *pmd1Δ* cells after growing for 4 h in YES medium at 32 °C – JBIR-141/Zn^{2+}, (**b**) Images of *pmd1Δ* cells after growing for 4 h in YES medium at 32 °C + JBIR-141/Zn^{2+}. Black bars represent 10 µm.

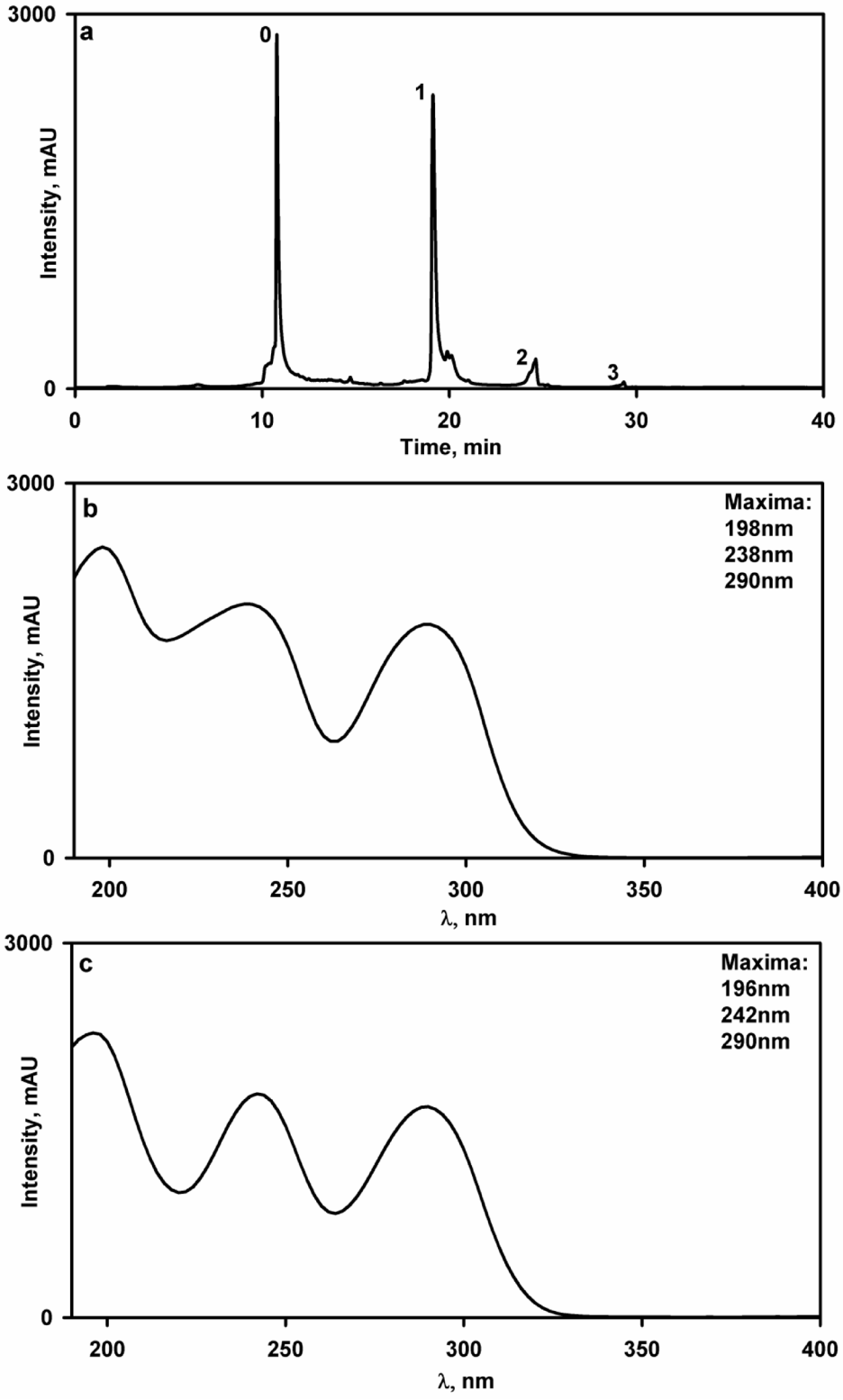

Fig. 2. HPLC and U.V. absorbance data. (**a**) HPLC trace (λ = 254 nm) of a sample of purified compound from S149. The four peaks obtained, Peaks 0–3, are labelled, (**b**):U.V. absorbance spectrum of Peak 0, (**c**) U.V. absorbance spectrum of Peak 1.

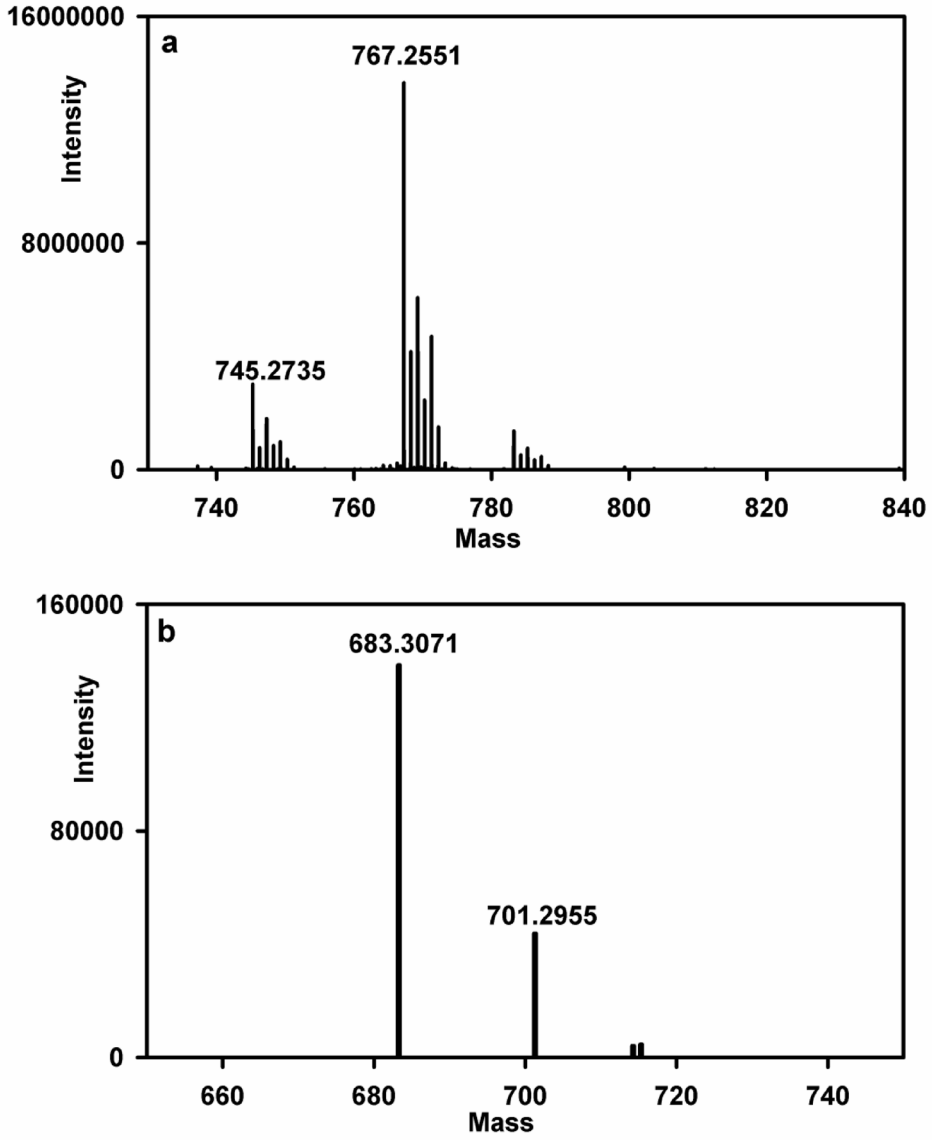

Fig. 3. Mass spectrometry data relating to the analysis of Peak 1. (**a**) MS data obtained when material from Peak 1 was analysed, (**b**) MS-MS mass spectrometry data obtained when the ~ $m/z = 745.2735$ $[M + H^+]$ ion from Peak 1 was analysed. The masses of the major ions are shown above the relevant peaks.

prediction/MS modelling tool based on $C_{31}H_{48}N_6O_{11}Zn_1$ $[H^+]$ (Fig. 5a and b). We also note the change in mass exhibited by the $m/z = 683.3614$ $[M + H^+]$ species when it forms the $m/z = 653.3655$ $[M + H^+]$ species suggested the loss of a nitroso group (-N = O) as the mass difference correlates exactly with the mass of this group (Fig. 4a and c).

Querying of the "Dictionary of Natural Products" (http://dnp.chemnetbase.com/faces/chemical/ChemicalSearch.xhtml) with the Zn^{2+} bound and Zn^{2+} unbound species accurate masses (744.2665 and 682.3544, respectively), did not identify any potential candidate molecules and it seemed *prima facie* that the molecule was novel. Material from Peak 1 was supplied to Fundacion Medina who, after confirming the MS data, calculated two possible molecular formulae, ($C_{30}H_{52}N_2O_{15}Zn$ & $C_{31}H_{48}N_6O_{11}Zn$), each comprising the zinc ion known to be present. Subsequently, 1 H NMR spectra were obtained by Fundacion Medina and several structural motifs identified which were used in database searches which resulted in the identification of the non-zinc bound 683.3614 $[M + H^+]$ species as JBIR-141 ($C_{31}H_{50}N_6O_{11}$). Although JBIR-141 was published in 2015[14] it had not been entered in the "Dictionary of Natural Products" (http://dnp.chemnetbase.com/faces/chemical/ChemicalSearch.xhtml) at the time of the present study (07-2017). Additional evidence supporting the proposed identification is JBIR-141 is a nitrosohydroxylamine compound [reviewed in[15]] which comprises a nitroso group, which we predicted from the MS data.

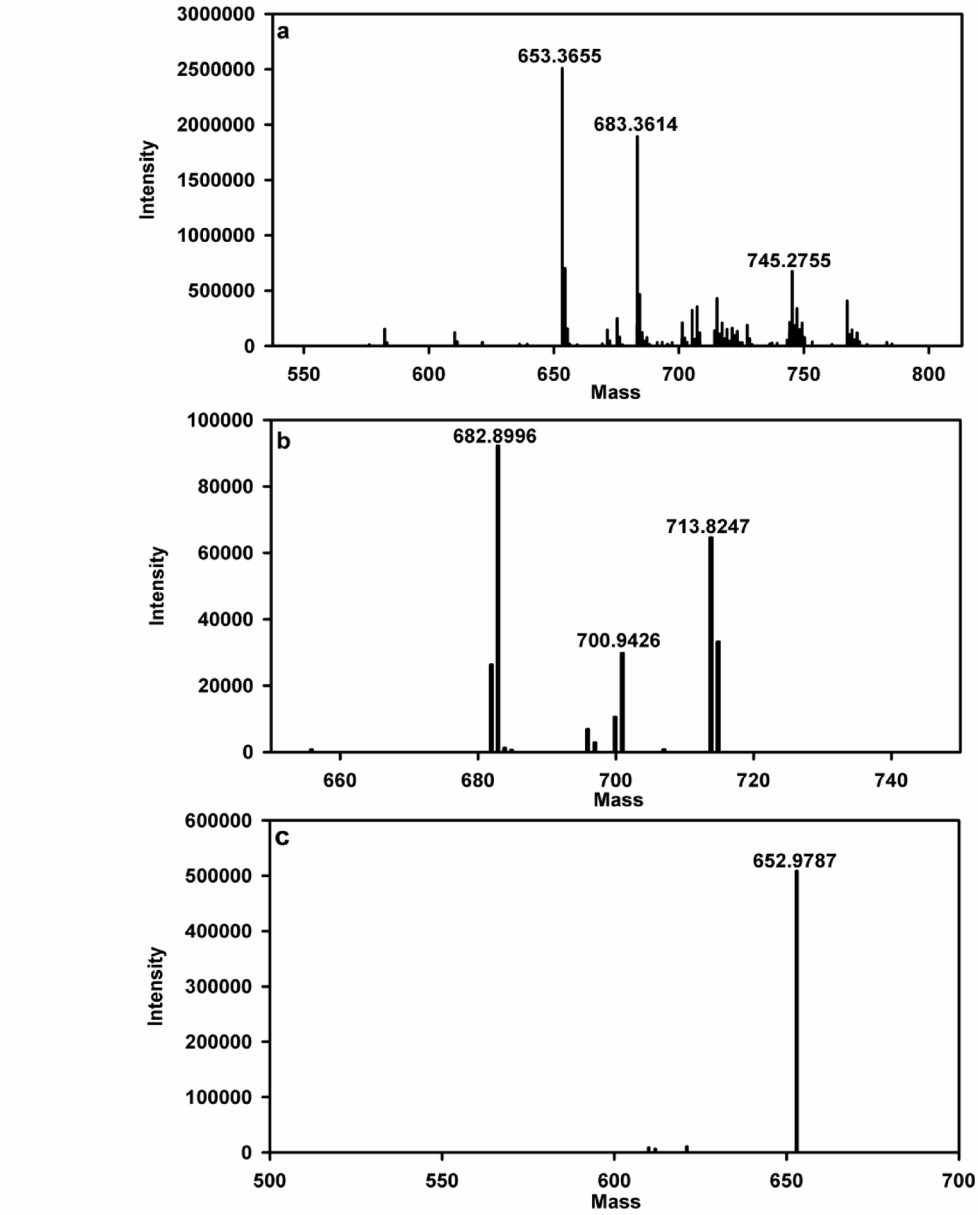

Fig. 4. Mass spectrometry data relating to the analysis of Peak 0. (**a**) MS data obtained when material from Peak 0 was analysed, (**b**) MS-MS mass spectrometry data obtained when the ~ $m/z = 745.2755$ $[M + H^+]$ ion from Peak 0 was analysed, (**c**) MS-MS mass spectrometry data obtained when the ~ $m/z = 683.3614$ $[M + H^+]$ ion from Peak 0 was analysed. The masses of the major ions are shown above the relevant peaks.

We note that neither JBIR-141 nor JBIR-142 (or any of their variants/ derivatives/ degradation products etc.) are described by Kawahara *et al.*., as binding, Zn^{2+}. It is possible the purification methods used by Kawahara *et al.*, stripped the Zn^{2+} from the molecules and their analyses were therefore conducted on the Zn^{2+} free forms. Acidic methanol has been shown to be capable of removing zinc ions from natural product complexes[16] and acidified solvents are described as being used by Kawahara *et al.*[14] . Acidified solvents were not used in the present study.

JBIR-141 as a zincophore

Compared to the number of iron binding natural products (siderophores) zincophores are relatively few in number. They include the porphyrin, zincphyrin (Fig. 6a][16], and the monocarboxylic acid ionophore zincophorin (Fig. 6b)[17,18], together with the closely related compounds griseochelin[19] and CP-78,545[20]. Zincophores also comprise several members of the nicotinianamine metallopine family[21,22], i.e. staphylopine[23,24], yersiniopine (Fig. 6c)[25], bacillopine and pseudopaline[26–28] and the more structurally diverse 2-hydroxyphenylthiazoline family which are characterised by possessing thiazolidine and/or thiazoline rings.

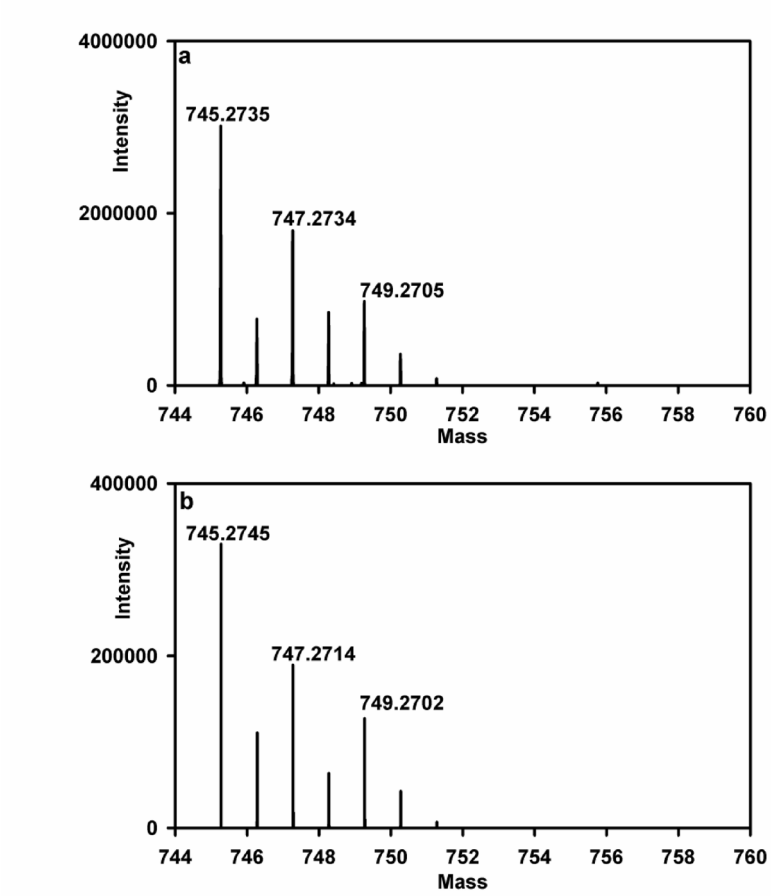

Fig. 5. Modelled and actual data relating to zinc derived isotope patterns. (**a**) MS data illustrating the modelled isotope profile of the $C_{31}H_{48}N_6O_{11}Zn_1$ $[H^+]$ ion, (**b**) MS data illustrating the isotope profile of the $m/z = 745.2735$ $[M + H^+]$ ion. The masses of the major ions are shown above the relevant peaks.

The 2-hydroxyphenylthiazoline family zincophores do not specifically bind zinc ions and often also form complexes with $Cu^{2+}$and Fe^{3+}. Transvalencin is considered to be a ferric iron binding siderophore, although it has also been shown to bind Zn^{2+} and Cu^{2+}[29,30] and yersiniabactin, (Fig. 6f) although well known as a siderophore, is also capable of binding Zn^{2+} and Cu^{2+} ions[31], tetrazolemycin is capable of binding Cu^{2+}, Zn^{2+} and Fe^{3+}[32], whilst micacocidin (Fig. 6e) has been shown to form complexes with Cu^{2+} (micacocidin B) and Fe^{3+} (micacocidin C), in addition to the dominant Zn^{2+} complexed form (micacocidin A)[33,34]. Coelibactin whose synthesis is induced by Zn^{2+}[35], may also be considered a zincophore, although this has not been demonstrated by purification of a coelibactin-Zn^{2+} complex. Pyochelin (Fig. 6d) is capable of binding Zn^{2+} and Fe^{3+}[36–38].

Pyochelin (Fig. 6d) is capable of binding Zn^{2+} although its affinity for Zn^{2+} is less than that for Fe^{3+}[39] and its affinity for iron is lower than for most siderophores[40,41]. Pyochelin binds Fe^{3+} with a 2:1 stoichiometry with one molecule of Pch tetradentately coordinated to Fe^{3+} and the second molecule bound bidentately to complete the octahedral geometry[42,43].

A crystal structure of the Zn^{2+} complexed form of micacocidin ("Micacocidin A") has been determined which allowed the Zn^{2+} coordinating atoms to be identified[34]. These are analogous to the atoms shown to coordinate Fe^{3+} in the yersiniabactin crystal structure[44].

A crystal structure of the Zn/Mg salt of zincophorin, the best studied monocarboxylic acid ionophore indicated chelation of the cation occurs octahedrally *via* the carboxylate and hydroxyls of C_{11} and C_{13} of two molecules of zincophorin[17]. Although complexation studies established a stability order of zinc ≈ cadmium > magnesium > strontium ≈ barium ≈ calcium for zincophorin[17] the affinity for iron and copper ions is unknown.

The groups involved in chelation of the zinc ion in JBIR-141 are unknown. However, the fact that two hydrogen ions are lost following zinc binding suggests that the oxygen atoms of the two hydroxyl groups in the molecule i.e. that of the nitrosohydroxylamine group and that linked to C_{24} of the tetramic acid moiety (Fig. 7a) are involved in coordination of the Zn^{2+}. The involvement of the oxygen atom of the hydroxyl group present in the nitrosohydroxylamine moiety in co-ordination of the Zn^{2+} is likely given its involvement in binding Cu^{2+} in cupferron[45] and dopastin[46].

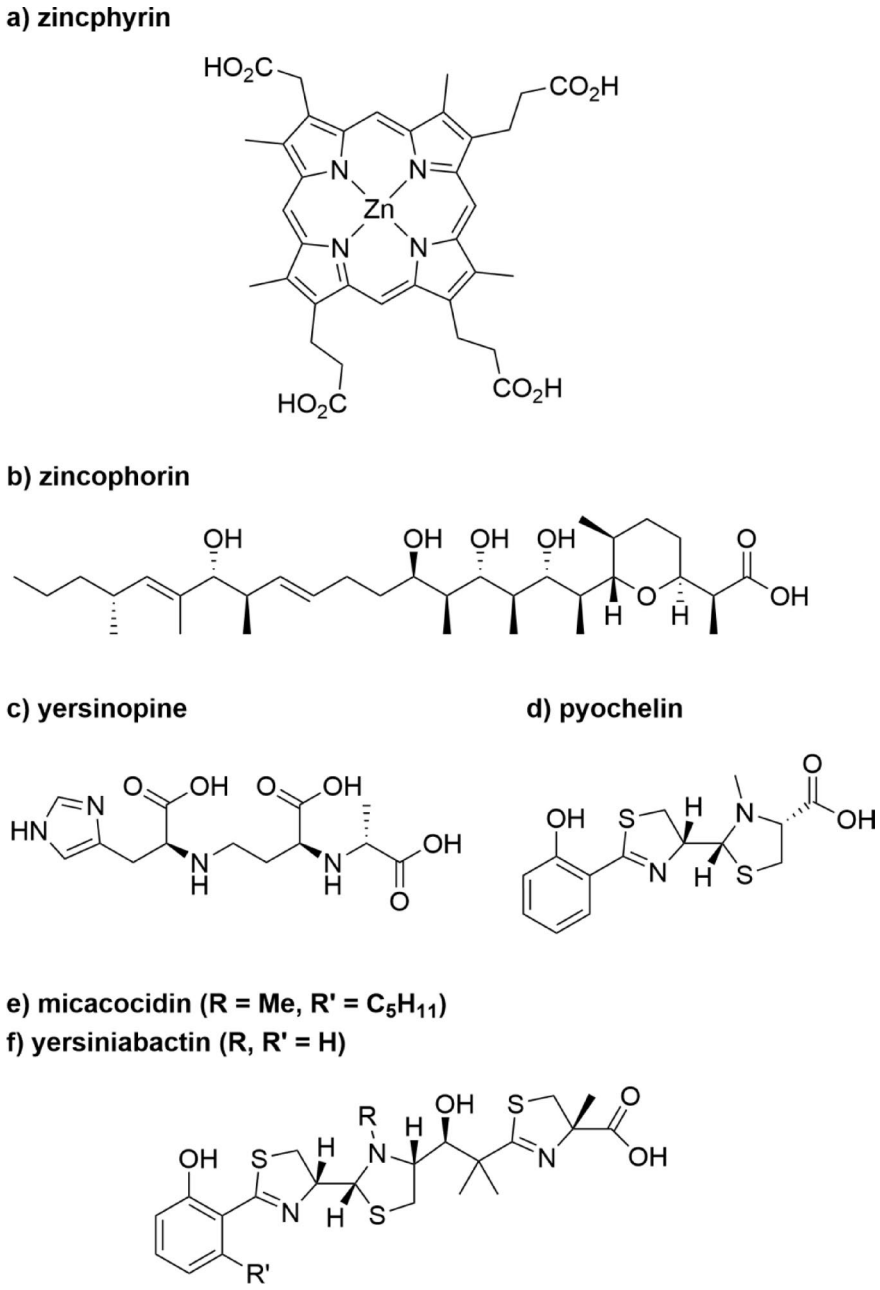

Fig. 6. Schematic diagrams of Zn^{2+} binding natural product compounds. (**a**) zincphyrin, (**b**) zincophorin, (**c**) yersiniopine, (**d**) pyochelin, (**e**) micacocidin, (**f**) yersiniabactin.

Although the structure of JBIR-141 (Fig. 7a), does not resemble the abovementioned zincophores (Fig. 6a–f) elements of its structure are analogous to those present in the well-studied siderophore mycobactin[47–49]. Mycobactin's structure (Fig. 7b) resembles that of JBIR-141 in that the centrally located, derivatised amino acid residue of both molecules is a basic one (in the case of myobactin, lysine, and in the case of JBIR-141, ornithine). Additionally, the modified amino acid residue with a cyclised side-chain located adjacent (N-terminally located) to the modified basic amino-acid residue is a hydroxylated one in both molecules (serine in the case of mycobactin and threonine in the case of JBIR-141). Moreover, we note both molecules are capable of binding metal ions (in the case of myobactin, Fe^{3+}, and in the case of JBIR-141, Zn^{2+}).

Identifying the target of JBIR-141 in *S. pombe*

JBIR-141 was identified during a screen for inhibitors of Foxo3a activity[14], although it is unclear from the available evidence whether it specifically targets the transcription factor itself, or an element of the upstream signalling cascade, for example AKT[14]. It is therefore difficult to extrapolate from this to explain the cell morphology phenotype observed in *S. pombe* in terms of the target of JBIR-141/Zn^{2+}. Of the three forkhead proteins in *S. pombe*, the only one involved in the mitotic cell cycle in fission yeast is *fkh2*. A *fkh2* deletion mutant is viable[50,51]

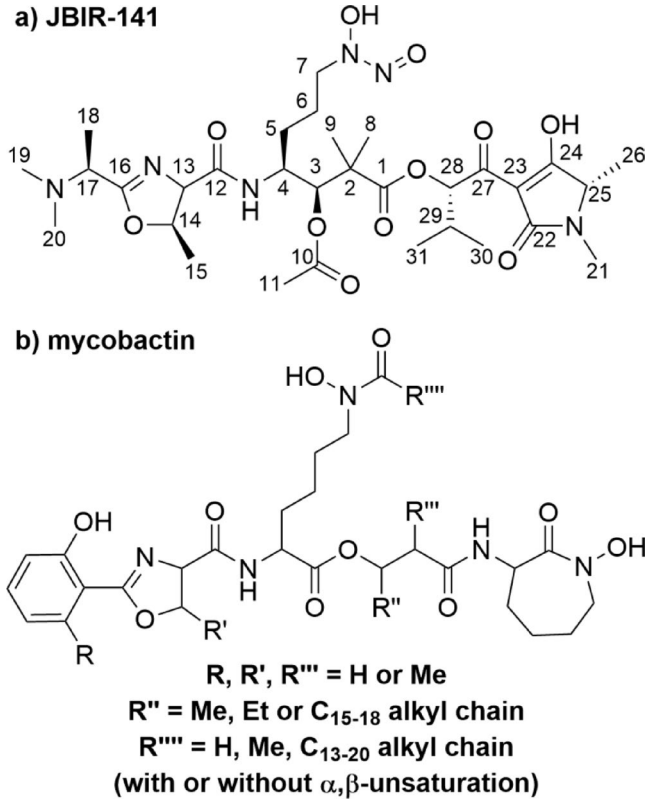

Fig. 7. Schematic diagrams of metal ion binding natural product compounds. (**a**) JBIR-141, (**b**) mycobactin.

and does not have a typical wee phenotype in fission yeast. It typically shows cells with different phenotypes such as misshapen and/or elongate cell phenotypes suggesting that it is not likely to be a major target of JBIR-141/Zn^{2+} in fission yeast given that JBIR-141/Zn^{2+} produces a wee cell phenotype.

To regulate entry into mitosis in all eukaryotes Cdk1 (Cdc2 in fission yeast) is regulated by the tyrosine kinase Wee1, which phosphorylates Cdc2 Y15 and inhibits mitotic entry and the tyrosine phosphatase Cdc25, which dephosphorylates the Y15 residue and activates entry into mitosis[52]. In the Cdc2 AF-Cdc13 fusion protein strain[53] T14 and Y15 have been mutated to A and F respectively and so cannot be tyrosine phosphorylated and thus are not regulated by Cdc25 and Wee1. This strain has a semi wee phenotype dividing on average at around 12 µm. To see if JBIR-141/Zn^{2+} was acting by affecting tyrosine 15 phosphorylation levels of Cdc2, and thus advancing cells into mitosis, we added JBIR-141/Zn^{2+} to the cdc2 AF mutant and found a further reduction in average cell size at mitosis (Fig. 8), showing that JBIR-141/Zn^{2+} was able to advance cells into mitosis. This suggests that JBIR-141/Zn^{2+} is not acting through Cdc2 tyrosine phosphorylation regulation to promote entry into mitosis.

As one way to identify the target of JBIR-141/Zn^{2+} we used viable deletion mutants that have a semi wee phenotype when deleted[11] (see Figs. 8 and 9 and "Experimental Procedures" 4.1 & 4.11–4.12). The mutants chosen were ones which generate viable healthy strains, as we did not wish the experiment to be complicated by poorly growing or "sick" strains in which the effects of JBIR-141 would be masked. Various combinations of these deletion mutants were smaller at cell division than each of the single mutants showing that these genes were acting in different pathways[11]. Using the single deletion mutants we reasoned that if addition of JBIR-141/Zn^{2+} did not alter cell size at division then the gene product may be a target of JBIR-141/Zn^{2+}, or the target gene product may act upstream or downstream in the same pathway, whereas, if the cell size at division is further reduced the gene product is unlikely to be a target of JBIR-141/Zn^{2+}. Each of the mutants was crossed into a *pmd1*Δ background and tested for a further reduction in cell size in the presence of JBIR-141/Zn^{2+} (see "Experimental Procedures" 4.1 & 4.11–4.12). All but one of the wee mutants tested showed a highly significant reduction (p-value $<<0.001$; one-tailed t-test) in cell size, of about ~ 10%, after addition of JBIR-141/Zn^{2+}. On this basis, their products or pathways are unlikely to be targets of JBIR-141/Zn^{2+} (Figs. 8 and 9 and Supplementary Table S1). However, the *pyp1* deletion mutant, did not show a significant reduction in cell size after addition of compound (p-value 0.10) (Figs. 8 and 9c,d and Supplementary Information Table S1), suggesting that Pyp1 is a direct target of JBIR-141/Zn^{2+}, or the target is in the same pathway as Pyp1.

The specific nature of this result also demonstrates that JBIR-141 is not exerting its phenotypic effect merely by perturbing homeostatic zinc levels within the cell, either by transporting additional Zn^{2+} into the cell or acting within the cell to sequester Zn^{2+}, but is presumably targeting a particular cellular component.

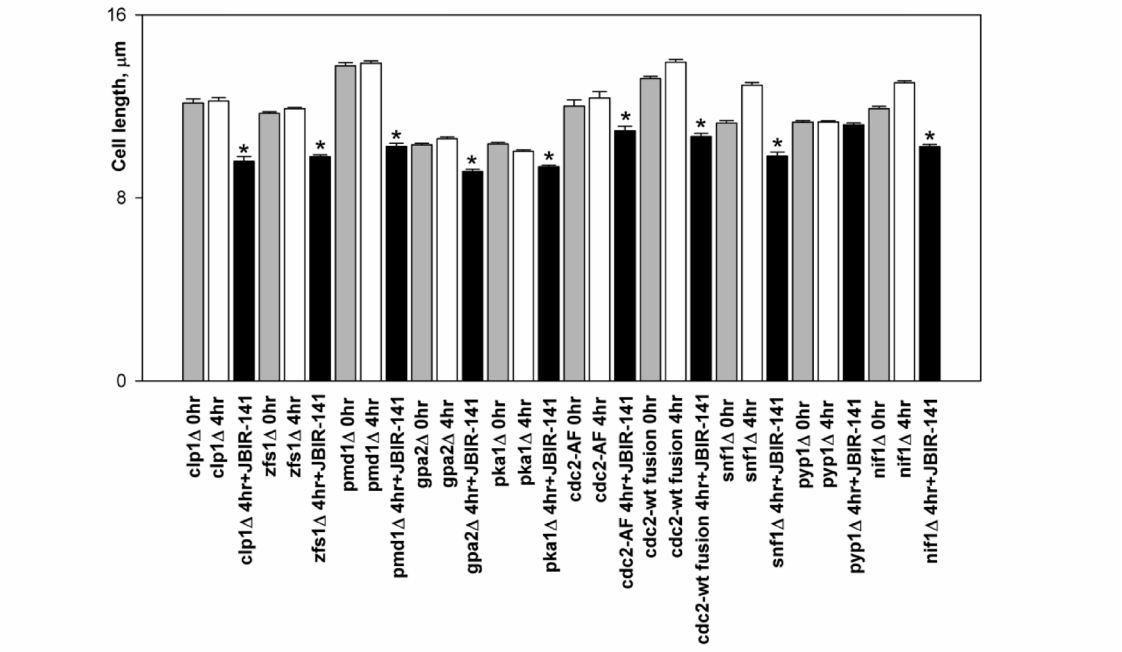

Fig. 8. Histograms illustrating the lengths of wee deletion mutant cells + or - JBIR-141/Zn^{2+}. The mutations *pyp1Δ*, *clp1Δ*, *zfs1Δ*, *gpa2Δ*, *pka1Δ*, *cdc2-AF-cdc13* (fusion), *cdc2-cdc13* (fusion), *snf1Δ* and *nif1Δ* are all in the *pmd1Δ* background. Grey bars represent cell lengths at 0 h prior to the 4 h treatment +/- JBIR-141/Zn^{2+}, white bars represent cell lengths after growing for 4 h in YES medium at 32 °C – JBIR-141/Zn^{2+} and black bars represent cell lengths after growing for 4 h in YES medium at 32 °C + JBIR-141/Zn^{2+}. * p-value for similarity of +/- JBIR-141/Zn^{2+} cell lengths < 0.05.

Pyp1 encodes a tyrosine phosphatase[54] and directly negatively regulates the Sty1 Map kinase which is involved in the Stress activated Map Kinase cascade[55]. Loss of Pyp1 activity rescues the loss of G2/M activator Cdc25 and activates entry into mitosis at a small cell size[56,57]. Pyp1 acts upstream of Cdc2 at mitosis and is implicated in regulation of Cdc2 tyrosine phosphorylation. However, although further work is needed to exclude alternative explanations the results shown here suggest Pyp1 may also be acting independently of Cdc2 tyrosine phosphorylation to advance cells into mitosis in the presence of S149.

Conclusion

The actinomycete strain S149 which induces a strong wee phenotype in fission yeast, was previously identified in a study where we described a novel screen for Actinomycete derived bioactive natural compounds using a microscopy-based approach, to determine their effect on *S. pombe* cellular morphology. Here we have identified the natural product compound synthesized by S149 which was responsible for inducing the phenotype as a novel zinc bound form of JBIR-141. JBIR-141 was not previously known to be a zincophore and does not share common structural motifs with the other known bacterial zincophores – mostly members of the 2-hydroxyphenylthiazoline family. By testing the effect of the Zn^{2+} bound form of JBIR-14 against a series of deletion mutants which express a wee phenotype we went on to show that JBIR-141/Zn^{2+} targets either the tyrosine phosphorylase Pyp1 itself, or an element in the same pathway. Further work is needed to determine whether JBIR-141/Zn^{2+} acts directly to accelerate mitotic entry in fission yeast, and other organisms.

Experimental procedures

Yeast strains, growth conditions and media

4.1 The actinomycete strain S149 was originally identified using the SAK950 strain (h + *ade6-M216*, *leu1-32*, *ura4-D18*, *caf5::bsdR*, *pap1Δ*, *pmd1Δ*, *mfs1Δ*, *bfr1Δ*, *dnf2Δ*, *erg5::ura4+*)[10]. Following analysis of each of these single mutants from the deletion collection[4] we found that a *pmd1Δ h* + was sufficient to make the yeast strains sensitive to S149 derived extracts. The deletion marker gene of *pmd1Δ* G418R[4] was replaced by Nat^R and the *pmd1Δ* Nat^R *h* + strain crossed to 972 h- to obtain a *pmd1Δ* Nat^R *h-* strain. This was crossed to each of the wee mutants to select for the wee genes in the *pmd1Δ* background (G418R Nat^R). All strains were grown at 32 °C in YE4S[58] except for crosses which were carried out on MEA agar plates.

Plug and filter paper assays

4.2 Pipette tips, (1 ml) were used to cut agar discs/plugs from confluent lawns of S149 cultured on Medium I agar (see below). The bacterial plugs, plus a control plug (agar-only), were placed at spaced out intervals on a YE4S plate seeded with 5×10^5 mid log phase *S. pombe* SAK950 cells. This procedure was generally carried out after intervals of 3, 5, 7 and 9 days of bacterial culture. The plates were incubated overnight at 30 °C and scored

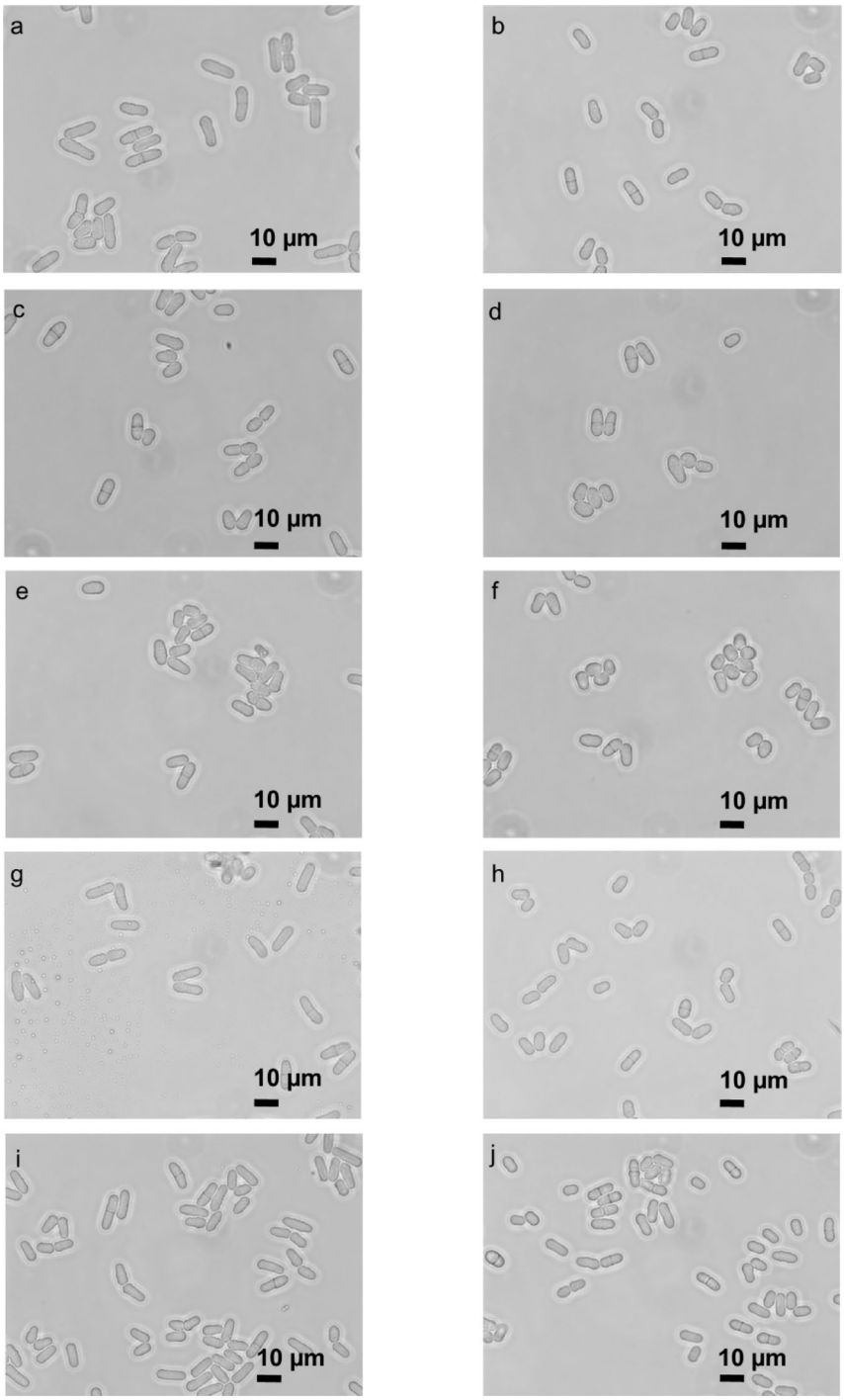

Fig. 9. Images illustrating the sizes of wee deletion mutant cells + or - JBIR-141/Zn^{2+}. Cells were grown for 4 h in YES medium at 32 °C before imaging. (**a**) *pmd1Δ* cells, no compound addition (**b**) *pmd1Δ* cells + JBIR-141/Zn^{2+} (**c**) *pyp1Δ* cells, no compound addition; (**d**) *pyp1Δ* cells + JBIR-141/Zn^{2+} (**e**) *gpa2Δ* cells, no compound addition; (**f**) *gpa2Δ* cells + JBIR-141/Zn^{2+} (**g**) *clp1Δ* cells, no compound addition (**h**) *clp1Δ* cells + JBIR-141/Zn^{2+} (**i**) *zfs1Δ* cells, no compound addition (**j**) *zfs1Δ* cells + JBIR-141/Zn^{2+}. Black bars represent 10 µm. All cultures were in exponential growth (OD_{595} 0.4–0.5) when photographed.

the following day for the presence/absence of a halo in the *S. pombe* lawns surrounding the plugs and, in the case of *S. pombe* SAK950, microscopically to assess the morphological appearance of the cells. As biomolecules can have differing effects at different concentrations, the morphological phenotype/s of the *S. pombe* cells was examined throughout the halo, from the plug to the halo edge.

Filter papers discs (Whatman Cat No: 2017-006), soaked in 10–30 µl of extract, or appropriate solvents used as negative controls, were used, in place of bacterial plugs, as described above.

Microscopy

4.3 Bright-field images of live cells were acquired on a Zeiss Axioskop 40 microscope equipped with a Zeiss 63X/1.4 oil ph3 objective and a Zeiss Axiocam MRm camera. For the plug assay plates cell images were captured with a Sony HD AVCHD camera using a Zeiss Akioskop 40 microscope equipped with a X50/0.56 Nikon objective and 2.5X optivar.

Bacterial strains, growth conditions and media

4.4 The study focussed on strain S149 which strongly inhibited the growth of *S. pombe* and induced the wee phenotype. The closest match to the 16 S rRNA sequence for S149 is *Streptomyces coeruleofuscus*, (GenBank: AB184840.1) with no mismatches out of 1,413 nucleotides of sequence. The physical characteristics of S149 are consistent with the published description of *Streptomyces coeruleofuscus*[13]. The strain was resuscitated from storage at -80 °C on oatmeal agar plates as described previously, and for spore production confluent bacterial lawns were streaked from the resuscitation plates on GYM agar plates and grown for 7 days at 30 °C[6]. Spores were prepared as described previously[59].

Production of aqueous bacterial cell extracts

4.5 S149 spores (~ 2,500 c.f.u. per plate) were streaked onto Medium I plates[9] produced from 25 l of Medium I agar and grown at 30 °C (usually 2–3 days) until they strongly produced JBIR-141/Zn^{2+}, as determined by assessing bioactivity using the "plug and filter paper assay". The plates were harvested in 1 l batches, the agar/mycelial mass disrupted by passaging through a 50 ml syringe and frozen separately at -20 °C.

Solvent extraction

4.6 The aqueous extract produced by squeezing the thawed agar/mycelial mass through muslin was extracted with an equal volume of petroleum ether and subsequently with five equal volumes of ethyl acetate. The ethyl acetate extracts were pooled, rotary evaporated to dryness using a standard Büchi rotary evaporator and the dried material was stored at -80 °C under nitrogen. The dried material was resuspended in 75 ml methanol which was added to 1,425 ml H_2O and then extracted with 2.7 l of dichloromethane (DCM).

Normal-phase flash chromatography and size exclusion chromatography

4.7 Fifteen grams of silica was added and the DCM rotary evaporated to dryness using a Büchi rotary evaporator. The silica with adsorbed S149 derived material was divided into two equal portions and each portion was transferred into a pre-packed disposable K-Sil 50 g column (Biotage) and used in normal-phase flash chromatography with elution in a 0-100% chloroform-methanol gradient using a Biotage "Isolera One" chromatography machine. Fractions containing bioactive compounds were identified by spotting 30 µl aliquots onto filter paper discs, which were used in the "plug and filter paper assay". Active fractions producing a halo of cells with the expected characteristic phenotypes were pooled and the methanol removed by a GeneVac Series II system equipped with a GeneVac VC3000TA condenser unit. The resultant sample was resuspended in 5 ml methanol and loaded onto a 150 PSI Max (Omnifit) size exclusion column packed with Sephadex™ LH-20 connected to a Biotage "Isolera One" chromatography machine and eluted in a methanol mobile phase (flow rate: 1 ml/min). Active fractions, identified by the "plug and filter paper assay" were pooled and the methanol removed using a GeneVac Series II system equipped with a GeneVac VC3000TA condenser unit. No acid was added to any of the solvents used in the purification procedure as this resulted in loss of bioactivity.

Reverse-phase flash chromatography

4.8 After resuspension in 20% methanol the sample was passed through a pre-packed "reverse phase" C18 Ultra 12 g "flash" chromatography column (Biotage) and the bound compounds eluted in a 20–100% water - methanol gradient using a Biotage "Isolera One" chromatography machine. Fractions containing bioactive compounds were identified by spotting 30 µl aliquots onto filter paper discs, which were used in the "filter paper assay". Active fractions producing a halo of cells with the expected characteristic phenotypes were pooled and the methanol removed by a GeneVac Series II system equipped with a GeneVac VC3000TA condenser unit. No acid was added to any of the solvents used in the purification procedure as this resulted in loss of bioactivity.

HPLC

4.9 All analyses/purifications were conducted as described previously[7], using an Agilent Technologies 1260 Infinity liquid chromatography machine equipped with either an Agilent Zorbax SB-C18 5 µM 4.6 × 150 mm column, a Waters Symmetry™ C18 4.6 × 250 mm column or an Agilent Eclipse Plus C18 3.5 µM 4.6 × 150 mm column equipped with a Hichrom C18 guard column JBIR-141/Zn^{2+} was eluted using a water – acetonitrile gradient over 30 min (10%-100% acetonitrile), with a flow rate of 1 ml min^{-1} and monitoring with a DAD array at λ = 210, 254, 273, 280, 300, 450 and 600 nm relative to λ = 360, and λ = 350 nm relative to λ = 500 nm. Fractions (0.5 ml) were collected in a 96 well block and active fractions identified by the "filter paper assay". Following correlation of peaks in the absorbance traces with the active fractions the method was repeated using an Agilent 1260 integrated fraction collector to "time-slice" and collect column eluate corresponding to the bioactive eluate into glass tubes. No acid was added to any of the solvents used as this resulted in loss of bioactivity.

Mass spectrometry

4.10 After removal of solvent using the GeneVac Series II and addition of 25% methanol to enhance solubility the samples were analysed by electrospray mass spectrometry (ESI-MS) using an LTQ-FT (Thermo) mass spectrometer with a 7T magnet at the Pinnacle Laboratory (Newcastle University), as described previously[7]. Experiments were run with a parent/precursor scan at 100,000 resolution. MS/MS fragmentations were carried

out in the ion-trap (LTQ) stage of the instrument. No acid was added to any of the solvents used as this resulted in loss of bioactivity.

Testing the effects of JBIR-141/Zn^{2+} on cell length

4.11 To examine the effect of JBIR-141/Zn^{2+} on the wee mutants, cells were grown in YE4S medium overnight to an $O.D._{595}$ = ~ 0.1–0.15, (Time 0 h) typically cultures were 5 ml. At Time 0 h cells samples were taken for % septation and cell length/width measurements. The culture was then split into two equal cultures (TEST and CONTROL) and purified JBIR-141/Zn^{2+} was added at 1/400 dilution of 10 mM stock in 96% ethanol to a final concentration of 25 μM to the TEST culture and equal volume of 96% ethanol to the CONTROL culture. Both cultures were incubated in a water bath at 32°C with shaking and samples for O.D., septation index and cell length were taken at 2 h and 4 h. Preliminary experiments showed that the effect of JBIR-141/Zn^{2+} began to be observed between 2–3 h and was maximal at 4 h.

Cell length measurements

4.12 Cells were imaged using a Zeiss Axioskop and 60X lens using Axiovision. The length and width of at least 50 septated cells were measured at each timepoint using Image J. The Excel function T.TEST (one-tailed; homoscedastic) was used to generate the *p*-values described in the text relating to Fig. 8.

Data availability

Data and materials relating to this study will be made available on request. Queries should be directed to Prof. J. Errington.

Received: 12 June 2025; Accepted: 6 October 2025
Published online: 12 November 2025

References

1. Mitchison, J. M. & Nurse, P. Growth in cell length in the fission yeast *Schizosaccharomyces Pombe*. *J. Cell. Sci.* **75**, 357–376 (1985).
2. Nurse, P. & Hayles, J. Using genetics to understand biology. *Heredity (Edinb)*. **123**, 4–13 (2019).
3. Wood, V. et al. The genome sequence of *Schizosaccharomyces Pombe*. *Nature* **415**, 871–880 (2002).
4. Kim, D. U. et al. Analysis of a genome-wide set of gene deletions in the fission yeast *Schizosaccharomyces Pombe*. *Nat. Biotechnol.* **28**, 617–623 (2010).
5. Hayles, J. et al. A genome-wide resource of cell cycle and cell shape genes of fission yeast. *Open. Biol.* **3**, 130053. https://doi.org/10.1098/rsob.130053.PMID (2013).
6. Lewis, R. A. et al. Screening and purification of natural products from actinomycetes that affect the cell shape of fission yeast. *J. Cell. Sci.* **130**, 3173–3185 (2017).
7. Lewis, R. A. et al. Screening and purification of natural products from actinomycetes that induce a rounded morphological phenotype in fission yeast. *Nat. Prod. Bioprospect.* **11**, 431–445 (2021).
8. Nurse, P. Fission yeast cell cycle mutants and the logic of eukaryotic cell cycle control. *Mol. Biol. Cell.* **31**, 2871–2873 (2020).
9. Kepplinger, B. *The Discovery And Characterisation Of novel Antibiotics From Amycolatopsis Isolate DEM30355* (University of Newcastle upon Tyne, 2016).
10. Aoi, Y. et al. Dissecting the first and second meiotic divisions using a marker-less drug hypersensitive fission yeast. *Cell. Cycle.* **13**, 1327–1334 (2014).
11. Navarro, F. J. & Nurse, P. A systematic screen reveals new elements acting at the G2/M cell cycle control. *Genome Biol.* **13**, R36. https://doi.org/10.1186/gb-2012-13-5-r36.PMID (2012).
12. Takai, A., Bialojan, C., Troschka, M. & Ruegg, J. C. Smooth muscle myosin phosphatase Inhibition and force enhancement by black sponge toxin. *FEBS Lett.* **217**, 81–84 (1987).
13. Trejo, W. H. & Bennett, R. E. Streptomyces species comprising the blue-spore series. *J. Bacteriol.* **85**, 676–690 (1963).
14. Kawahara, T. et al. Foxo3a inhibitors of microbial origin, JBIR-141 and JBIR-142. *Org. Lett.* **17**, 5476–5479 (2015).
15. Blair, L. M. & Sperry, J. Natural products containing a nitrogen-nitrogen bond. *J. Nat. Prod.* **76**, 794–812 (2013).
16. Toriya, M. et al. Zincphyrin, a novel coproporphyrin III with zinc from *Streptomyces Sp*. *J. Antibiot.* **46**, 196–200 (1993).
17. Brooks, H. A., Gardner, D. & Poyser, J. P. The structure and absolute stereochemistry of Zincophorin (antibiotic M144255): a monobasic carboxylic acid ionophore having a remarkable specificity for divalent cations. *J. Antibiot.* **37**, 1501–1503 (1984).
18. Walther, E. et al. Zincophorin – biosynthesis in streptomyces griseus and antibiotic properties. *GMS Infect. Dis.* **4** (Doc08). https://doi.org/10.3205/id000026 (2016).
19. Gräfe, U., Schade, W. & Roth, M. Griseochelin, a novel carboxylic acid antibiotic from *Streptomyces griseus*. *J Antibiot*. **37**, 836–846 (1984).
20. Dirlam, J. P. et al. CP-78,545, a new Monocarboxylic acid ionophore antibiotic related to Zincophorin and produced by a *Streptomyces*. *J. Antibiot.* **42**, 1213–1220 (1989).
21. Morey, J. R. & Kehl-Fie, T. E. Bioinformatic mapping of opine-like Zincophore biosynthesis in bacteria. *mSystems* **5**, e00554–e00520 (2020).
22. McFarlane, J. S., Davis, C. L. & Lamb, A. L. Staphylopine, Pseudopaline and Yersinopine dehydrogenases: a structural and kinetic analysis of a new functional class of opine dehydrogenases. *J. Biol. Chem.* **293**, 8009–8019 (2018).
23. Ghssein, G. et al. Biosynthesis of a broad-spectrum nicotianamine-like metallophore in Staphylococcus aureus. *Science* **362**, 1105–1108 (2016).
24. Grim, K. P. et al. The metallophore Staphylopine enables *Staphylococcus aureus* to compete with the host for zinc and overcome nutritional immunity. *mBio* **8**, e0128–e0117 (2017).
25. Chabaan, T., Mohsen, Y., Ezzeddine, Z. & Ghssein, G. Overview of *Yersinia pestis* metallophores: Yersiniabactin and Yersinopine. *Biology* **12** https://doi.org/10.3390/biology12040598 (2023).
26. Gi, M. et al. A novel siderophore system is essential for the growth of *Pseudomonas aeruginosa* in airway mucus. *Sci. Rep.* **5**, 14644. https://doi.org/10.1038/srep14644 (2015).
27. Mastopasqua, M. C. et al. Growth of *Pseudomonas aeruginosa* in zinc poor environments is promoted by a nicotianamine-related metallophore. *Mol. Microbiol.* **106**, 543–561 (2017).
28. Ghssein, G. & Ezzeddine, Z. Review of Pseudomonas aeruginosa metallophores: pyoverdine, Pyochelin and Pseudopaline. *Biology* **11**, 1711. https://doi.org/10.3390/biology11121711 (2022).
29. Hoshino, Y. et al. Transvalencin A, a Thiazolidine zinc complex antibiotic produced by a clinical isolate of *Nocardia transvalensis*. I Taxonomy, Fermentation, isolation and biological activities. *J. Antibiot.* **57**, 797–802 (2004).

30. Hoshino, Y. et al. Transvalencin A, a Thiazolidine zinc complex antibiotic produced by a clinical isolate of *Nocardia transvalensis*. II. Structure Elucidation. *J. Antibiot.* **57**, 803–807 (2004).
31. Bobrov, A. G. et al. The yersinia pestis siderophore, yersiniabactin, and the ZnuABC system both contribute to zinc acquisition and the development of lethal septicaemic plague in mice. *Mol. Microbiol.* **93**, 759–775 (2014).
32. Liu, N., Shang, F., Xi, L. & Huang, Y. Tetrazolemycins A and B, two new oxazole-thiazole siderophores from deep sea *Streptomyces Olivaceus* FXJ8.012. *Mar. Drugs*. **11**, 1524–1533 (2013).
33. Kobayashi, S. et al. B and C, novel Antimycoplasma agents from *Pseudomonas sp*. I. Taxonomy, fermentation, isolation, physico-chemical properties and biological activities. *J. Antibiot.* **51**, 323–327 (1998).
34. Kobayashi, S. et al. Micacocidin A, B and C, novel Antimycoplasma agents from *Pseudomonas sp*. II structure Elucidation. *J. Antibiot.* **51**, 328–332 (1998).
35. Kallifidas, D. et al. The zinc-responsive regulator Zur controls expression of the coelibactin gene cluster in *Streptomyces coelicolor*. *J. Bacteriol.* **192**, 608–611 (2010).
36. Namiranian, S., Richardson, D. J., Russell, D. A. & Sodeaqu, J. R. Excited state properties of the siderophore Pyochelin and its complex with zinc ions. *Photochem. Photobiol.* **65**, 777–782 (1997).
37. Cuppels, D. A., Stipanovic, R. D., Stoessl, A. & Stothers, J. B. The constitution and properties of a pyochelin-zinc complex. *Can. J. Chem.* **65**, 2126–2130 (1987).
38. Brandel, J. et al. Pyochelin, a siderophore of *Pseudomonas aeruginosa*: physicochemical characterization of the iron (III), copper (II) and zinc (II) complexes. *Dalton Trans.* **41**, 2820–2834 (2012).
39. Braud, A., Geoffrey, V., Hoegy, F., Mislin, G. L. A. & Schalk, I. J. Presence of the siderophores Pyoverdine and Pyochelin in the extracellular medium reduces toxic metal accumulation in *Pseudomonas aeruginosa* and increases bacterial metal tolerance. *Environ Microbiol Rep.* **2**, 419–425 (2010).
40. Cox, C. D., Jnr, R. & Moore, K. L. M. L. & Carter Cook Jnr, C. Pyochelin: novel structure of an iron-chelating growth promoter for *Pseudomonas aeruginosa*. *Proc. Natl. Acad. Sci. U. S. A.* **78** 4256–4260. (1981).
41. Yang, B., Hoegy, F., Mislin, G. L. A., Mesini, P. J. & Schalk, I. J. Terbium, a fluorescent probe for investigation of siderophore Pyochelin interactions with its outer membrane transporter FptA. *J. Inorg. Biochem.* **105**, 1293–1298 (2011).
42. Tseng, C-F. et al. Bacterial siderophores: the solution stoichiometry and coordination of the Fe(III) complexes of Pyochelin and related compounds. *J. Bio Inorg. Chem.* **11**, 419–432 (2006).
43. Cobessi, D., Celia, H. & Pattus, F. Crystal structure at high resolution of ferric-pyochelin and its membrane receptor FptA from *Pseudomonas aeruginosa*. *J. Mol. Biol.* **352**, 893–904 (2005).
44. Miller, M. C., Parkin, S., Fetherston, J. D., Perry, R. D. & DeMoll, E. Crystal structure of ferric-yersiniabactin, a virulence factor of *Yersinia pestis*. *J. Inorg. Biochem.* **100**, 1495–1500 (2006).
45. Heyn, A. H. & Dave, N. G. Precipitation of metal-cupferron complexes from homogeneous solution-I: determination of copper. *Talanta* **13**, 27–32 (1966).
46. Shiino, M., Watanabe, Y. & Umezawa, K. Synthesis of N-substituted N-nitrosohydroxylamines as inhibitors of mushroom tyrosinase. *Bioorg. Med. Chem.* **5**, 1233–1240 (2001).
47. Snow, G. A. The structure of mycobactin P, a growth factor for *Mycobacterium johnei*, and the significance of its iron complex. *Biochem. J.* **94**, 160–165 (1965).
48. Fang, Z., Sampson, S. L., Warren, R. M., van Gey, N. C. & Newton-Foot, M. Iron acquisition strategies in mycobacteria. *Tuberculosis (Edinb)*. **95**, 123–130 (2015).
49. Quadri, L. E., Sello, J., Keating, T. A., Weinreb, P. H. & Walsh, C. T. Identification of a *Mycobacterium tuberculosis* gene cluster encoding the biosynthetic enzymes for assembly of the virulence-conferring siderophore mycobactin. *Chem. Biol.* **5**, 631–645 (1998).
50. Bulmer, R. et al. The forkhead transcription factor Fkh2 regulates the cell division cycle of *Schizosaccharomyces Pombe*. *Eukaryot. Cell.* **3**, 944–954 (2004).
51. Buck, V. et al. Fkh2p and Sep1p regulate mitotic gene transcription in fission yeast. *J. Cell. Sci.* **117**, 5623–5632 (2004).
52. Gould, K. L. & Nurse, P. Tyrosine phosphorylation of the fission yeast cdc2 + protein kinase regulates entry into mitosis. *Nature* **342**, 39–45 (1989).
53. Coudreuse, D. & Nurse, P. Driving the cell cycle with a minimal CDK control network. *Nature* **468**, 1074–1079 (2010).
54. Ottilie, S., Chernoff, J., Hannig, G., Hoffman, C. S. & Erikson, R. L. A fission-yeast gene encoding a protein with features of protein-tyrosine-phosphatases. *Proc. Natl. Acad. Sci. U. S. A.* **88**, 3455–3459 (1991).
55. Shiozaki, K., Shiozaki, M. & Russell, P. Mcs4 mitotic catastrophe suppressor regulates the fission yeast cell cycle through the Wik1-Wis1-Spc1 kinase cascade. *Mol. Biol. Cell.* **8**, 409–419 (1997).
56. Millar, J. B., Russell, P., Dixon, J. E. & Guan, K. L. Negative regulation of mitosis by two functionally overlapping PTPases in fission yeast. *EMBO J.* **11**, 4943–4952 (1992).
57. Ottilie, S., Chernoff, J., Hannig, G., Hoffman, C. S. & Erikson, R. L. The fission yeast genes *pyp1* + and *pyp2* + encode protein tyrosine phosphatases that negatively regulate mitosis. *Mol. Cell. Biol.* **12**, 5571–5580 (1992).
58. Moreno, S., Klar, A. & Nurse, P. Molecular genetic analysis of *Schizosaccharomyces Pombe*. *Methods Enzymol.* **194**, 795–823 (1991).
59. Kieser, T., Bibb, M. J., Buttner, M. J., Chater, K. F. & Hopwood, D. A. *Practical Streptomyces Genetics* (The John Innes Foundation, 2000).

Acknowledgements

We thank Dr B. Hover and Dr N. Dales of Odyssey Therapeutics Inc for permission to publish and J. Devi for scientific discussions.

Author contributions

RAL and JH did the experimental work, analysed and interpreted the data and wrote the manuscript. MJH provided scientific advice. JG assisted with the mass spectrometry and the interpretation of MS data. SM and JL provided technical assistance to JH. NEEA and JE managed the project. All authors have read and approved the manuscript.

Funding

Ongoing funding in the Errington lab is funded by an ARC Australian Laureate Fellowship grant (number FL210100071).

Declarations

Competing interests

The authors have no competing interests. RAL, NEEA and JE hold shares, or share options, in Demuris Ltd/ Odyssey Therapeutics Inc.

Additional information

Supplementary Information The online version contains supplementary material available at https://doi.org/10.1038/s41598-025-23271-w.

Correspondence and requests for materials should be addressed to R.A.L.

Reprints and permissions information is available at www.nature.com/reprints.

Publisher's note Springer Nature remains neutral with regard to jurisdictional claims in published maps and institutional affiliations.